Journal of Electroceramics 4:2/3, 279–287, 2000

The Effect of Size, Strain, and Long-Range Interactions on Ferroelectric Phase Transitions in $KTaO_3/KNbO_3$ Superlattices Studied by X-ray, EXAFS, and Dielectric Measurements

H.-M. CHRISTEN & K.S. HARSHAVARDHAN
Neocera, Inc., 10000 Virginia Manor Road, Suite 300, Beltsville MD 20705

M.F. CHISHOLM, E.D. SPECHT, J.D. BUDAI, D.P. NORTON & L.A. BOATNER
Oak Ridge National Laboratory, Oak Ridge, TN 37831

I.J. PICKERING
Stanford Synchrotron Radiation Laboratory/SLAC, Stanford CA 94309

Abstract. Epitaxial, uniformly strained superlattices of ferroelectric $KNbO_3$ and paraelectric $KTaO_3$ are studied with respect to their structural and dielectric properties. For dielectric measurements, perfectly lattice-matched conducting $Sr(Ru_{0.5}Sn_{0.5})O_3$ electrodes are used, and a broad, frequency-dependent maximum is observed in the capacitance-vs-temperature curves. Niobium K-edge glancing-angle EXAFS provides information regarding the crystal structure of $KNbO_3$ films as thin as two unit cells in superlattices with equal $KTaO_3$ and $KNbO_3$ layer thicknesses, showing a clear difference between these thinnest-layer superlattices and films of the $K(Ta_{0.5}Nb_{0.5})O_3$ solid-solution. X-ray diffraction measurements, on the other hand, indicate that these samples exhibit the same transition temperature T_c, indicating the importance of long-range electrostatic interactions. Analysis of the transition temperature for various structures leads to a clear identification of the effect of size and strain on T_c.

Keywords: ferroelectrics, superlattices, size effects, strain effects, potassium niobate ($KNbO_3$)

Introduction

The study of size effects in ferroelectrics is complicated in most experiments by the coexistence of intrinsic (''true'' size effects) and extrinsic effects. The latter includes defects, surface charges, surface tensions, non-uniform strains, and the influence of electrodes. These extrinsic effects complicate the interpretation of experimental results obtained on free-standing wedge-shaped samples [1,2], fine-grained ceramics [3,4], and epitaxial thin films [5].

In the current work, these difficulties are circumvented by the special properties of epitaxial superlattices consisting of alternating layers of paraelectric $KTaO_3$ and ferroelectric $KNbO_3$ grown on (0 0 1)-oriented $KTaO_3$ substrates. The lattice mismatch between these two materials is in fact small enough to allow the formation of misfit-free structures, resulting in a uniform and thickness-independent strain throughout these structures. This clearly distinguishes these samples from the similar perovskite superlattices studied earlier [6–8].

This paper focuses on new EXAFS experiments, dielectric measurements, and Z-contrast transmission electron microscopy, and compares the results to those from x-ray diffraction studies published earlier [9,10]. It is thus intended to provide a comprehensive overview of the phenomena observed in $KTaO_3/KNbO_3$ superlattices and to show how size effects, strain effects, and long-range interactions can be identified and isolated in this simple physical system.

All superlattices studied in this work were grown with equal $KTaO_3$ and $KNbO_3$ thicknesses, and all samples had approximately the same total thickness. In the following, a structure consisting of, e.g., 50 repetitions of a stacking of 4 unit cells of $KTaO_3$ and 4 unit cells of $KNbO_3$, will be referred to as a 4/4 structure, etc.

Experimental Methods

Niobium K-edge extended X-ray absorption fine structure (EXAFS) data were collected at the Stanford Synchrotron Radiation Laboratory on beamline 6–2 using a Si(1 1 1) double crystal monochromator. Incident intensity was measured using an Ar-filled ion chamber and the Nb K-edge EXAFS was collected by monitoring the Nb K_α fluorescence using a 13-element germanium detector. The films were maintained at a glancing angle of approximately 5° in order to optimize the signal from niobium while minimizing surface effects. Upstream apertures were used to reduce the beam size to less than that of the sample. For a K-absorption edge, the contribution of an atom-atom vector to the EXAFS has a cosine-squared relationship with the angle between that vector and the X-ray electric vector [11]. Therefore, for each structure two measurements were made, with the *e*-vector either in the plane of the structure or normal to it. EXAFS data were extracted according to conventional methods, using the EXAFSPAK program suite [12]. EXAFS curve fitting was carried out using fixed coordination numbers assuming a distorted perovskite model and refining interatomic distances and Debye-Waller factors. Phase and amplitude functions were calculated using the program feff [13]. The accuracy of interatomic distances is estimated to be $\pm$ 0.01 Å.

Dielectric measurements were carried out using a Hewlett-Packard 4284A impedance analyzer at frequencies from 10 Hz to 1 MHz. Gold pads were *e*-beam evaporated through a shadow mask both onto the superlattice and onto the epitaxial $Sr(Ru_{0.5}Sn_{0.5})O_3$ bottom-electrode, and gold wires were attached to these pads using silver epoxy. The measurements were performed in air.

Z-contrast scanning electron transmission microscopy (STEM) [14] was used to image the samples with atomic resolution for [1 0 0] zone axis oriented cross-sectioned samples. In these micrographs, the positions of the Ta, Nb, Sr, and (Ru_xSn_{1-x}) columns can be clearly distinguished and located directly from the image.

Room-temperature X-ray diffraction measurements were performed using a rotating-anode Cu K_α X-ray source, a vertically focusing LiF monochromator, and a flat Ge analyzer crystal. For the temperature-dependent X-ray experiments, Ge crystals were used both as monochromator and analyzer. The samples were mounted on a flat heater plate using silver paint and kept in air.

Growth of $KNbO_3/KTaO_3$ Superlattices, $K(Ta_xNb_{1-x})O_3$ Solid-Solution Films, and $Sr(Ru_xSn_{1-x})O_3$ Bottom Electrodes

$KNbO_3$, $KTaO_3$, and $K(Ta_{0.5}Nb_{0.5})O_3$ films have been grown onto $KTaO_3$ substrates by pulsed laser deposition (PLD), using the ''segmented target'' method first proposed by Yilmaz et al. [15] A KNO_3 segment acts as an extra potassium-source to compensate for this material's high volatility. The stoichiometry of the films was verified using Rutherford Backscattering (RBS) [16]. For the growth of $K(Ta_xNb_{1-x})O_3$, the target was further segmented to incorporate $KTaO_3$ and $KNbO_3$ ''wedges'' [17] in the correct proportions. $KTaO_3$ substrates were cut from spontaneous-nucleation grown boules and were polished using a KOH-buffered colloidal silica slurry. Contrary to the case of $SrTiO_3$ or $LaAlO_3$, a high-temperature anneal (800°C, 10 min) of these surfaces in oxygen (100 mTorr) results in atomically flat terraces with a single termination. This was verified by atomic force microscopy (AFM), revealing only 4 Å steps [18].

The growth rates for $KTaO_3$ and $KNbO_3$ were calibrated from test samples on which the thickness was determined by X-ray superlattice reflections and transmission electron microscopy (TEM). The growth rates depended most critically on the target density. With hot-pressed ceramics having a density of at least 98% of the theoretical value, the growth rates for $KTaO_3$ and $KNbO_3$ were found to be identical to within experimental accuracy. The $K(Ta_{0.5}Nb_{0.5})O_3$ films were grown from a segmented target containing an equal amount of $KTaO_3$ and $KNbO_3$ and thus have exactly the same average composition as the superlattices.

For dielectric measurements, epitaxial conducting bottom electrodes were used. It was crucial to find a conducting oxide with a lattice constant precisely equal to that of the $KTaO_3$ substrates in order not to change the amount of strain in the superlattices. A solid-solution of the metallic perovskite $SrRuO_3$ (pseudocubic with $a = 3.930$ Å, i.e., smaller than $KTaO_3$ with $a = 3.989$ Å) and the insulating perovskite $SrSnO_3$ (double-perovskite unit cell with $a = 2 \times 4.033$ Å) results in a metastable semiconducting oxide $Sr(Ru_xSn_{1-x})O_3$. For $x = 0.5$, the lattice constant matches that of the $KTaO_3$ substrate. In fact, no misfit dislocations could be found in cross-sectional TEM images of $Sr(Ru_{0.5}Sn_{0.5})O_3/KTaO_3$ interfaces. *Z*-contrast STEM was further used to image the samples with atomic resolution. The results are shown in Fig. 1, demonstrating that the interfaces are atomically flat. This type of image was also used to calibrate the growth rates of $KTaO_3$ and $KNbO_3$, and all further superlattices were grown with equal $KTaO_3$ and $KNbO_3$ thicknesses.

Typical growth conditions for $KTaO_3$, $KNbO_3$, $K(Ta_{0.5}Nb_{0.5})O_3$, and $Sr(Ru_{0.5}Sn_{0.5})O_3$ films were: substrate temperature 770°C; oxygen pressure, 100 mTorr; target-substrate distance 6 cm; laser energy density 1.5 J/cm^2; and pulse repetition rate 3.3 Hz.

Properties of Bulk $KNbO_3$

The crystal structure of bulk $KNbO_3$ has been studied in great detail [19]. At high temperatures, $KNbO_3$ is a cubic perovskite with a paraelectric-to-ferroelectric phase transition at 435°C, below which a tetragonal phase is observed. The ferroelectric polarization, as well as the Nb-displacement with respect to the rigid oxygen octahedron, are along the pseudocubic $[0\,0\,1]_{pc}$ directions. At 225°C, $KNbO_3$ becomes orthorhombic with the Nb-displacement now parallel to $[0\,1\,1]_{pc}$, and at -108°C, a transition to the lowest-temperature rhombohedral phase is observed in which the Nb-displacement and the ferroelectric polarization are along the $[1\,1\,1]_{pc}$ directions.

At room temperature, $KNbO_3$ is orthorhombic (Amm2) with $a = 3.973$ Å (parallel to the pseudocubic $[1\,0\,0]_{pc}$), $b = 5.695$ Å (parallel to $[0\,\overline{1}\,1]_{pc}$), and $c = 5.721$ Å (parallel to $[0\,1\,1]_{pc}$).

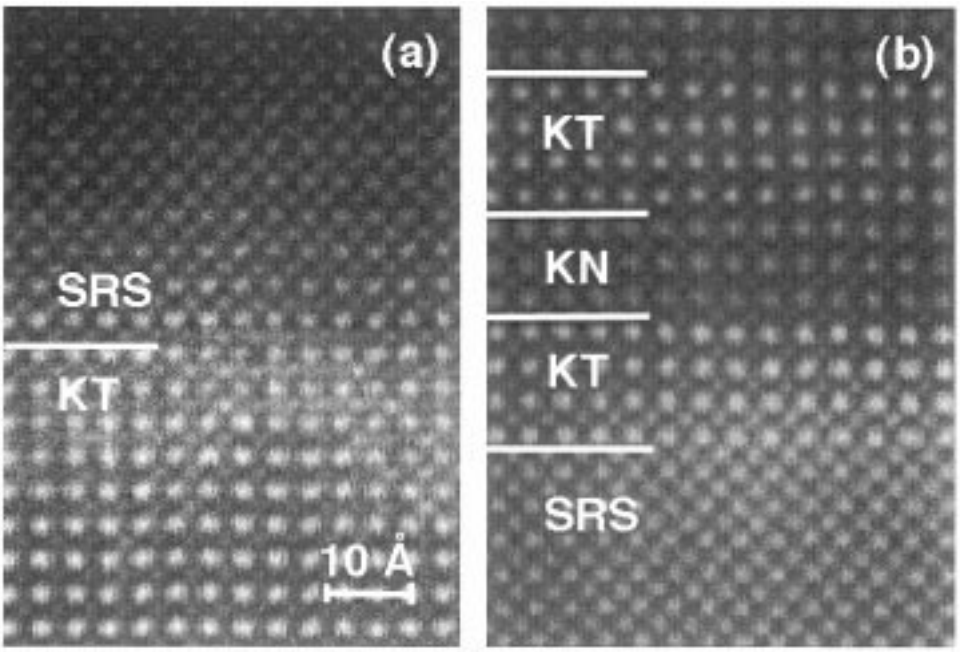

Fig. 1. Scanning transmission electron micrographs of (a) a $Sr(Ru_{0.5}Sn_{0.5})O_3$ film on a $KTaO_3$ substrate, and (b) a $KTaO_3/KNbO_3$ superlattice on a $Sr(Ru_{0.5}Sn_{0.5})O_3$ electrode film. No misfit dislocations are observed, indicating the perfect lattice match between all (clamped) layers and the substrate.

X-ray Study of $KNbO_3$ Films

X-ray normal $\theta-2\theta$ scans of $KNbO_3$ films on $KTaO_3$ substrates are consistent with the bulk structure for film thicknesses greater than 1 μm. With the (0 1 1) orientation [i.e., the pseudocubic $(0\,0\,1)_{pc}$] normal to the substrate, this structure results in a lattice mismatch of only 0.4%. This mismatch is considerably smaller than the value of 2.2% observed in the $SrTiO_3/BaTiO_3$ system studied earlier by others [20,21].

As a consequence of the small lattice mismatch, misfit dislocations are not likely to form immediately at the film/substrate interface, and it is expected that thinner films are more strongly strained than these thick layers.

This assumption is confirmed by a structural analysis of 1700 Å-thick layers. Here, a different type of orthorhombic structure is observed with $a = 3.975$ Å and $b = 4.001$ Å in the plane of the substrate and $c = 4.055$ Å in the normal direction. Interestingly, the film's [h h 0] or [h $\bar{\text{h}}$ 0] directions are parallel to an in-plane substrate $\langle \text{h h } 0 \rangle$ axis, rather than the a and b axes aligning with the $\langle \text{h } 0\,0 \rangle$ axes of the substrate. Note that for this new orthorhombic structure observed for the thin films, $(a+b)/2$ equals 3.988, which results in an even better lattice match (well below 0.1%) with $KTaO_3$.

Even thinner films were analyzed in superlattice structures, because single films would result in X-ray reflections that are too weak to be analyzed accurately. Films with layer thicknesses below 160 Å were thus studied in superlattices with a total thickness of 1700 Å, and in which the $KTaO_3$ and $KNbO_3$ individual-layer thicknesses were equal.

Within experimental accuracy, these thinner films do not exhibit the split peaks of the orthorhombic structures. The observed peaks are consistent with a tetragonal structure, with (0 0 1) normal to the surface and [1 0 0] aligned with the substrate [1 0 0]. Superlattice satellites were easily observed on structures with individual layer thicknesses of 1, 2, 4, 6, 13, and 42 unit cells. Figure 2 shows the results for 42/42 structure.

From these superlattice peaks, the periodicity Λ can be determined accurately. However, neither the relative thickness of the two layers nor the atomic layer spacing in either material are determined by this measurement, as they will only affect the intensities of the reflections. Nevertheless, from the known stacking of the structures and the temperature variation of the periodicity $\Lambda(T)$, the variation of the average normal lattice constant can be determined. This approach will be used below to observe phase transitions.

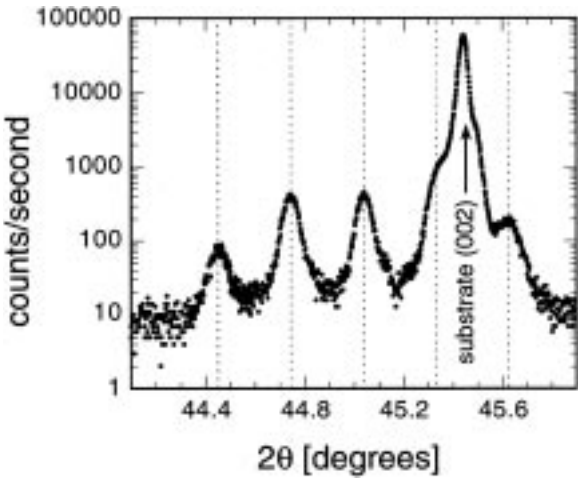

Fig. 2. Normal $\theta-2\theta$ x-ray scan for a superlattice in which the $KTaO_3$ and the $KNbO_3$ layers are each 42 unit cells thick. The position of the substrate reflection is also indicated.

Results of EXAFS Measurements

X-ray diffraction is sensitive to the entire superlattice and essentially probes the average structure. In contrast, the Nb-edge EXAFS experiment probes the Nb environment only. Two superlattices were analyzed, namely the 2/2 and 42/42 structures, as well as the $K(Ta_{0.5}Nb_{0.5})O_3$ solid-solution film.

Within experimental error, the superlattices showed identical Nb-Nb and Nb-O distances in the plane of the substrate [$d^{\text{in}}{}_{SL}$(Nb-Nb) = 3.99 Å, $d^{\text{in}}{}_{SL}$(Nb-O) = 1.91 Å and 2.10 Å]. Out of the plane, the Nb-Nb and Nb-O distances are different from the in-plane values, but again no distinction can be made between the 2/2 and the 42/42 structures [$d^{\text{norm}}{}_{SL}$(Nb-Nb) = 4.03 Å, $d^{\text{norm}}{}_{SL}$(Nb-O) = 1.84 Å and 2.20 Å].

Unfortunately, the data was insufficient to determine with certainty the spacegroup of the material. Clearly the data does not fit a simple tetragonal structure. In fact, the Nb-ion appears to be displaced from its high-symmetry position. Assuming that this displacement is confined to a plane described by the

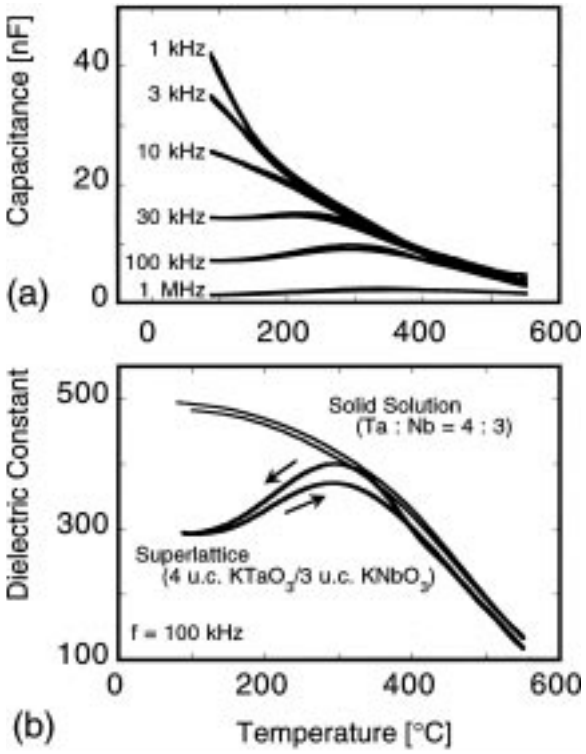

Fig. 3. (a) Capacitance measured on the $KTaO_3/KNbO_3$ superlattice (4/3 structure) of Fig. 1 using an epitaxial $Sr(Ru_{0.5}Sn_{0.5})O_3$ bottom electrode. Data obtained both on heating and cooling are shown for various frequencies. (b) 100 kHz data from (a) replotted in terms of the dielectric constant and compared to data obtained on a solid-solution of the same average composition (curves obtained upon heating and cooling are shown).

pseudocubic $[1\,1\,0]_{pc}$ and $[0\,0\,1]_{pc}$ directions (which is the plane containing the Nb-displacement in all phases of bulk $KNbO_3$), simple geometric considerations yield a displacement of about 0.38 Å along $[1\,1\,0]_{pc}$ and 0.18 Å along $[0\,0\,1]_{pc}$.

For the $K(Ta_{0.5}Nb_{0.5})O_3$ film, data analysis was complicated by the equal number of Nb and Ta nearest neighbors for each Nb ion. Nevertheless, it was clearly observed that the Nb-O distances were slightly smaller than in the superlattices and that the two values for d_{SS}(Nb-O) were closer to each other than those of the superlattice. This indicates a smaller Nb-displacement in $K(Ta_{0.5}Nb_{0.5})O_3$ than in the superlattices. Also observed was a clear increase in the normal Nb-Nb/Ta distances [$d^{norm}{}_{SS}$(Nb-Nb) and $d^{norm}{}_{SS}$(Nb-Ta)] as compared to the superlattices.

To summarize, EXAFS results reveal no measurable differences in the local Nb-environment between the 2/2 and 42/42 samples. The $KNbO_3$ in these two superlattices thus appears to exhibit the same crystalline structure. In contrast, the $K(Ta_{0.5}Nb_{0.5})O_3$ solid-solution film showed a distinctively different local Nb-environment. This indicates that a 2/2 superlattice is structurally identical to superlattices with larger periodicities, but different from a solid-solution.

Strain Effects and Size Effects

The combined results of X-ray diffraction, EXAFS, and STEM demonstrate clearly that for individual layer thicknesses up to 42 unit cells, the $KTaO_3/KNbO_3$ superlattices are uniformly strained. The perfect ''clamping'' of the films to the substrate results in a large strain—large enough, in fact, to promote the formation of a crystalline structure that is different from that observed in the bulk. The films relax to the bulk structure only when the film thickness is almost two orders of magnitude larger than that of any of the films in the superlattices studied here. Most important is the fact that this novel crystalline structure is identical in all of the superlattices studied in this work. In other words, these superlattices allow us to vary the thickness of the layers without varying the amount of strain or changing the crystalline structure of the material. Strain effects, therefore, are observed on all structures in the same way, whereas differences in the behavior of the various superlattices can only be attributed to the varying thicknesses of the $KTaO_3$ and $KNbO_3$ layers. To the best of the authors' knowledge, this is the only physical system in which the distinction between size and strain can be made this clearly and without having to consider extrinsic effects such as surface charges, surface tension, electrode effects, defects, and nonuniformities in composition and/or strain.

Dielectric Measurements

Dielectric measurements were performed using the epitaxial bottom electrodes described above. The results obtained for the structure of Fig. 1 are shown in Fig. 3(a). The capacitance was measured from room temperature to 500°C, and only a weak difference was observed between the data obtained on heating and on cooling. In Fig. 3(b), the data obtained at 100 kHz is

replotted in terms of the dielectric constant (as calculated from the capacitance, film thickness, and top electrode surface area) and compared to that obtained on a solid-solution film of the same average composition. The solid-solution data exhibit a very weak frequency dependence, contrary to the case of the superlattice, where a marked decrease of the capacitance with increasing frequency is seen. For neither the superlattice nor the solid-solution does the capacitance-vs-temperature data show any distinctive peaks. This result is contrary to the case of $K(Ta_{0.5}Nb_{0.5})O_3$ films grown by the same method on $SrRuO_3$[17]. In those $K(Ta_{0.5}Nb_{0.5})O_3/SrRuO_3$ structures, the lattice mismatch between the electrode and the dielectric film is sufficiently large to promote the formation of misfit dislocations, resulting in relaxed (i.e., not strained) $K(Ta_{0.5}Nb_{0.5})O_3$ films, indicating that the observed behavior is directly related to the large strain. A somewhat similar behavior has been observed for $SrTiO_3/BaTiO_3$ superlattices [22] when the total thickness of the superlattice was kept below a critical value, but additional work is needed to clarify this issue.

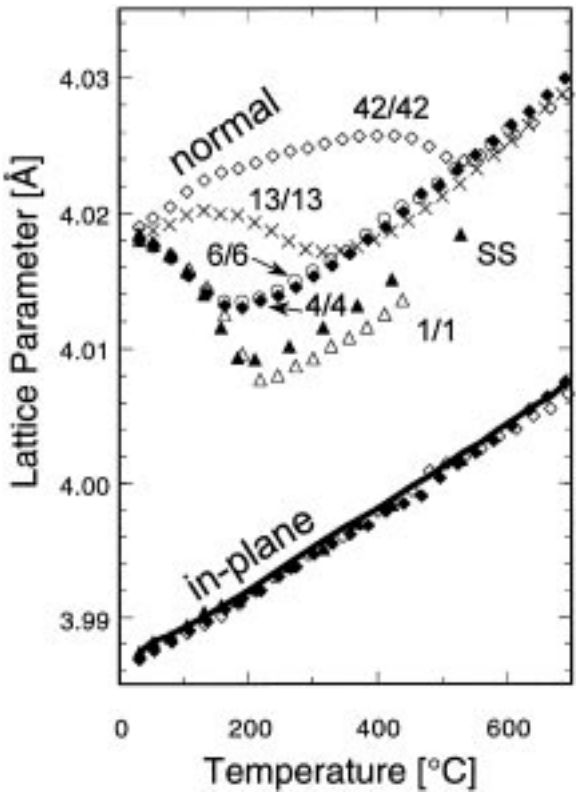

Fig. 4. Lattice parameter of the $KTaO_3/KNbO_3$ superlattices obtained on cooling. Data is shown for the following structures: 42/42 (◇), 13/13 (×), 6/6 (○), 4/4 (◆), and 1/1 (△), as well as the solid-solution (▲). For clarity, the in-plane lattice parameter is shown only for the 42/42 and 4/4 structures. The solid line indicates the substrate lattice parameter.

Structural Phase Transition and Size Effect

As noted above, X-ray diffraction experiments readily determine the superlattice period Λ, from which the average $KTaO_3/KNbO_3$ lattice parameter's temperature dependence can be observed. Figure 4 shows the results for both the in-plane and normal lattice parameters for temperatures from 20°C to 700°C. Clearly, all of the in-plane lattice parameters mimic that of the substrate, confirming the above assumption of perfectly ''clamped'' films.

A clear change of sign in the normal thermal expansion coefficient is observed for all superlattices and for the solid-solution, signaling a structural phase transition. No thermal hysteresis is observed. T_c is taken as the highest temperature where the thermal expansion changes sign and is plotted as a function of $KNbO_3$ layer thickness in Fig. 5.

Thinner $KNbO_3$ films clearly undergo a phase transition at much lower temperatures than the thicker ones. A decrease of T_c with decreasing size is expected from free-energy considerations for a ferroelectric slab with domains in which the polarization is normal to the surface. In this case, for a slab of thickness t with domains of size D, the free energy F of the thin slab is given by [23]

$$F(T) = F_{\text{bulk}}(T) + \sigma_{\text{wall}}/D + a\,D/t \qquad (1)$$

In this expression, $F_{\text{bulk}}(T)$ describes the temperature dependence of F in the bulk material, the second term represents the energy of the domain walls, and the third term is the electrostatic energy resulting from the fields penetrating into the space surrounding the slab. As the thickness decreases, this last term increases, making it favorable to form smaller domains. Wang et al. [24] have performed numerical simulations to predict how this affects the transition temperature. In their model, the function $T_c(t)$ is given in terms of two empirical parameters, namely the transition temperature $T_c(\text{inf})$ of an infinitely thick slab, and a correlation length t_c at which $T_c(t_c) = 0$. A

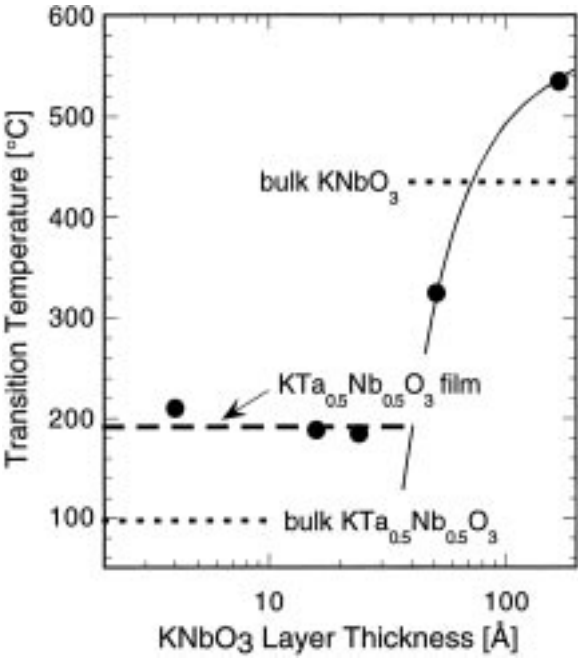

Fig. 5. Transition temperature as a function of $KNbO_3$ layer thickness. The broken line indicates the transition temperature of the solid-solution film. Also shown are the transition temperatures of bulk $KNbO_3$ and $KTa_{0.5}Nb_{0.5}O_3$. The thin solid line indicates the type of behavior expected from [24].

sketch of this $T_c(t)$ dependence is shown in Fig 5. Clearly, the available data does not allow us to determine the relevant parameters. For argument's sake, the curve was drawn with $T_c(\text{inf}) = 620°\text{C}$ and $t_c = 18\,\text{Å}$.

Long-range Interactions

It is clearly observed in Fig. 5 that the behavior described by Eq. (1) does not fit the experimental data for the thinner layers. Two effects compete as the layers become thinner in these $KTaO_3/KNbO_3$ superlattices. First, as both $KTaO_3$ and $KNbO_3$ layers are varied simultaneously, the interaction between the individual $KNbO_3$ layers increases as their separation decreases. In the simplest model, this interaction is determined by the fields produced by the domains, and these fields fall off exponentially at distances that are large compared to the domain size.

The domain size D is thus a critical length scale describing the interaction between layers, and a decrease in D will compete with the increase in the layer-layer coupling as the superlattice periodicity is reduced. However, Eq. (1) imposes a decrease of D as $t^{1/2}$ (cf. [24]). In other words, the domain size decreases less rapidly than the layer thickness, and there will be a thickness below which $D > t$, resulting in the fields originating from the domains in one $KNbO_3$ layer to penetrate into the next one.

Using the above estimates of $T_c(\text{inf})$ and t_c used to draw the $T_c(t)$ line in Fig. 5, the predictions of Wang's model show that for 70 Å thick $KNbO_3$ films, the domain size equals the layer thickness. In other words, for $KNbO_3$ layer thicknesses well below 17 unit cells, the behavior of the superlattice is determined by collective phenomena and mimics that of the solid-solution.

In order to fully understand the behavior of these structures at small thicknesses, a model must take into consideration the entire superlattice geometry, rather than treating the layers as individual entities. Schwenk et al. [25] have proposed an approach which considers a multilayer system consisting of two soft-mode-driven ferroelectrics with different transition temperatures. (Note that $KTaO_3$ can be regarded as a soft-mode type ferroelectric with a hypothetical transition temperature low enough to be suppressed by zero-point fluctuations [26].) The results of a Ginzburg-Landau functional calculation indicate that with decreasing thickness of the individual layers, the transition temperature decreases and converges to a finite value, as is also found in numerical simulations treating the system as a transverse Ising model [27].

Superlattices vs. Solid-Solution Films

As observed in Fig. 5, the transition temperature of a $K(Ta_{0.5}Nb_{0.5})O_3$ solid-solution is equal to that of superlattices in which the $KNbO_3$ layer thickness is less than about 6 unit cells. Quite surprisingly, however, there are distinct structural differences between these superlattices and the solid-solution, as revealed by the EXAFS measurements discussed above. This indicates that the temperature at which the material ceases to be ferroelectric is determined by long-range electrostatic interactions, whereas the structure of the ferroelectric phase itself is dictated by the local environment.

Strain Effects

As discussed above, the strain in all structures investigated here is identical. It is, therefore, expected that the effect of this strain will be similar for all samples. Inspection of Fig. 5 confirms this assumption. Transition temperatures approximately 100°C above the bulk values are observed both in the solid-solution layers and the thickest $KNbO_3$ films (films in which the size-effects are the weakest, yet which are thin enough so that the entire sample is uniformly strained. Thicker, relaxed $K(Ta_xNb_{1-x})O_3$ films exhibit bulk-like transition temperatures [17]).

A T_c of 190°C is measured for the solid-solution film (compared to the bulk value of 93°C) [28], and $T_c = 535$°C for the 42/42 structure (compared to 435°C for bulk $KNbO_3$).

Simple arguments suffice to explain this increase of T_c in $KNbO_3$. At the transition temperature of bulk $KNbO_3$ (435°C), the substrate lattice parameter is $a = 4.000$ Å (from Fig. 4). Using published values for the lattice constant of cubic and tetragonal $KNbO_3$ [19], and assuming a similar thermal expansion for $KNbO_3$ as for $KTaO_3$ (again from Fig. 4), one finds for $KNbO_3$ at 435°C, $a_{\text{cubic}} = 4.005$ Å and $a_{\text{tetragonal}} = 4.002$ Å. Because the tetragonal structure is a better match to the $KTaO_3$ substrate, the ''clamping'' to the substrate will tend to stabilize the low-temperature phase above the bulk phase transition.

The fact that two-dimensional compression results in an increase in T_c has been confirmed experimentally and explained by a thermodynamic formalism in (Ba,Sr)TiO_3 [29] and Pb(Zr,Ti)O_3 [30] thin films.

Conclusions

The $KTaO_3/KNbO_3$ superlattices studied here by STEM, X-ray diffraction, dielectric measurements, and EXAFS, have proven to be excellent systems for the study of size effects, strain effects, and long-range ferroelectric interactions. These phenomena can be observed separately due to the unique uniformly strained state of the films resulting from the small lattice mismatch between the two materials. More work is required on superlattices in which the thicknesses of the $KTaO_3$ and $KNbO_3$ layers are varied separately. Nevertheless, for structures with equal $KTaO_3$ and $KNbO_3$ thicknesses, the following conclusions arise:

1. For $KTaO_3/KNbO_3$ superlattice periodicities below ~ 90 unit cells, the crystalline structure and the amount of stress are independent of the layer thickness.
2. Dielectric measurements on such superlattices reveal a broad, frequency-dependent maximum in the $\varepsilon(T)$ curves.
3. X-ray diffraction experiments indicate a sharp phase transition, contrary to the dielectric measurements.
4. The strain in these structures results in an increase of the transition temperature by about 100°C.
5. Decreasing the thickness of the $KNbO_3$ layers results in a decrease of the transition temperature, consistent with a model that predicts the disappearance of ferroelectricity in $KNbO_3$ layers with thicknesses below ~ 20 Å. This disappearance is not observed as long-range interactions become dominant at smaller periodicites.
6. At periodicities below ~ 60 Å, the transition temperature of the superlattices becomes equal to that of the solid-solution.
7. The room-temperature crystalline structures (as observed by EXAFS) of a 2/2 superlattice and a solid-solution film are distinctively different, even though they exhibit the same transition temperature.
8. In these strained $KNbO_3$ films, the direction of the Nb displacement lies between those observed in the bulk orthorhombic and rhombohedral phases.

Acknowledgments

The authors would like to acknowledge the invaluable contributions of J.A. Kolopus, J.T. Luck, J.O. Ramey, L.A. Gea, P. Menchhofer, and P.J. Marrero. Part of this work was supported by the Division of Materials Sciences, U.S. Department of Energy under Contract No. DE-AC-96OR22462, and the ORNL Postdoctoral Research Associates Program. The Stanford Synchrotron Radiation Laboratory (SSRL) is funded by the Department of Energy, Office of Basic Energy Sciences, Divisions of Chemical and Materials Science. The Biotechnology Program is supported by the National Institutes of Health, National Center for Research Resources, Biomedical Technology Program. Further support is provided by the Department of Energy, Office of Biological and Environmental Research.

References

1. F. Tsai and J.M. Cowley, *Appl. Phys. Lett*., **65**, 1906 (1994).
2. S.B. Ren, C.J. Lu, J.S. Liu, H.M. Shen, and Y.N. Wang, *Phys. Rev*., **B54**, R14337 (1996).
3. P. Ayyub, V.R. Palkar, S. Chattopadhyay, and M. Multani, *Phys Rev*., **B51**, 6135 (1995); S. Chattopadhyay, P. Ayyub, V.R. Palkar, and M. Multani, *ibid*., **52**, 13177 (1995).
4. M.H. Frey and D.A. Payne, *Appl. Phys. Lett*., **63**, 2753 (1993).
5. Y. Yano, K. Iijima, Y. Daitoh, T. Terashima, and Y. Bando, *J. Appl. Phys*., **76**, 7833 (1994).
6. H. Tabata and T. Kawai, *Appl. Phys. Lett*., **70**, 321 (1997).
7. A. Erbil, Y. Kim, and R.A. Gerhardt, *Phys. Rev. Lett*., **77**, 1628 (1996).
8. I. Kanno, S. Hayashi, R. Takayama, and T. Hirao, *Appl. Phys. Lett*., **68**, 328 (1996).
9. H.-M. Christen, E.D. Specht, D.P. Norton, M.F. Chisholm, and L.A. Boatner, *Appl. Phys. Lett*., **72**, 2535 (1998).
10. E.D. Specht, H.-M. Christen, D.P. Norton, and L.A. Boatner, *Phys. Rev. Lett*., **80**, 4317 (1998).
11. I.J. Pickering, and G.N. George, *Inorganic Chemistry*, **34**, 3142 (1995).
12. http://www-ssrl.slac.stanford.edu/exafspak.html
13. J.J. Rehr, J. Mustre de Leon, S.I. Zabinsky, S.I., R.C. Albers, *J. Am. Chem. Soc*., **113**, 5135 (1991).
14. S.J. Pennycook and D.E. Jesson, *Phys. Rev. Lett*., **64**, 938 (1990).
15. S. Yilmaz, T. Venkatesan, and R. Gerhard-Mulhaupt, *Appl. Phys. Lett*., **58**, 2479 (1991).
16. H.-M. Christen, L.A. Boatner, J.D. Budai, M.F. Chisholm, L.A. Gea, P.J. Marrero, and D.P. Norton, *Appl. Phys. Lett*., **68**, 1488 (1996).
17. H.-M. Christen, D.P. Norton, L.A. Gea, and L.A. Boatner, *Thin Solid Films*, **312**, 156 (1998).
18. H.-M. Christen, L.A. Boatner, J.D. Budai, M.F. Chisholm, L.A. Gea, D.P. Norton, Ch. Gerber, and M. Urbanik, *Appl. Phys. Lett*., **70**, 2147 (1997).
19. A.W. Hewat, *J. Phys. C: Solid State Phys*., **6**, 2559 (1973).
20. E. Wiener-Avnear, *Appl. Phys. Lett*., **65**, 1784 (1994).
21. H. Tabata, H. Tanaka, and T. Kawai, *Appl. Phys. Lett*., **65**, 1970 (1994).
22. B.D. Qu, M. Evstigneev, D.J. Johnson, and R.H. Prince, *Appl. Phys. Lett*., **72**, 1394 (1998).
23. M.E. Lines and A.M. Glass, *Principles and Applications of Ferroelectrics and Related Materials* (Clarendon Press, Oxford, 1977), pp. 94–96.
24. Y.G. Wang, W.L. Zhong, and P.L. Zhang, *Phys. Rev*., **B51**, 5311 (1995).
25. D. Schwenk, F. Fishman, and F. Schwabl, *Phys. Rev*., **B38**, 11618 (1988); *J. Phys.: Condens. Matter*, **2**, 5409 (1990).
26. U.T. Höchli and L.A. Boatner, *Phys Rev*., **B20**, 266 (1979).
27. B.D. Qu, W.L. Zhong, and P.L. Zhang, *Phys. Lett*., **A189**, 419 (1994); *Jpn. J. Appl. Phys*., **34**, 4114 (1995).
28. D. Rytz and H.J. Scheel, *J. Cryst. Growth*, **59**, 468 (1982).
29. I.N. Zakharchenko, E.S. Nikitin, V.M. Mukhortov, Yu.I. Golovko, M.G. Radchenko, and V.P. Dukdevich, *Phys. Stat. sol.(a)*, **114**, 559 (1989).
30. S. Hoon Oh and Hyun M. *Jang, Appl. Phys. Lett*., **72**, 1457 (1999).